Experimental Cell Research 443 (2024) 114311

Contents lists available at ScienceDirect

Experimental Cell Research

journal homepage: www.elsevier.com/locate/yexcr

Research article

Epigenetic modulation of vascular calcification: Looking for comprehending the role of sirt1 and histone acetylation in VSMC phenotypic transition

Geórgia da Silva Feltran [a], Emerson Araújo Alves dos Santos [a], Amanda Fantini de Camargo Andrade [a], Willian Fernando Zambuzzi [a,**], Rodrigo Augusto Foganholi da Silva [b,c,*]

[a] Lab. of Bioassays and Cellular Dynamics, Department of Chemical and Biological Sciences, Institute of Biosciences, UNESP – São Paulo State University, 18618-970, Botucatu, São Paulo, Brazil
[b] Program in Environmental and Experimental Pathology, Paulista University, São Paulo, 04026-002, São Paulo, Brazil
[c] Graduate Program in Health Sciences, University of Taubaté, Taubaté, SP, 12020-340, Brazil

ARTICLE INFO

Keywords:
Vascular smooth muscle cells (VSMCs)
Epigenetic regulation
Vascular calcification
SIRT1
Histone acetylation

ABSTRACT

In light of the complex origins of ectopic vascular calcification and its significant health implications, this study offers a comprehensive exploration of the molecular dynamics governing vascular smooth muscle cells (VSMCs). Focusing on epigenetic modulation, we investigate the transition from a contractile to a calcifying phenotype in VSMCs, with an emphasis on understanding the role of SIRT1. For this purpose, a single batch of human aortic SMCs, used at a specified passage number to maintain consistency, was subjected to calcium and phosphate overload for up to 72 h. Our findings, validated through RT q-PCR, Western blot, immunofluorescence, and DNA methylation analyses, reveal a complex interplay between acetyltransferases and deacetylases during this phenotypic transition. We highlight HAT1A's critical role in histone acetylation regulation and the involvement of HDACs, as evidenced by subcellular localization studies. Moreover, we demonstrate the modulation of SIRT1 expression, a class III deacetylase, during VSMC calcification, underscoring the influence of DNA methylation in this process. Importantly, the study addresses previously unexplored aspects of the dynamic protein expression patterns observed, providing insight into the counterintuitive expressions of key proteins such as Runx2 and osterix. This research underscores the significant impact of epigenetic mechanisms, particularly the modulation of SIRT1, in the transition from a contractile to a calcifying phenotype in VSMCs, offering potential avenues for further exploration in the context of vascular calcification.

1. Introduction

The vascular smooth muscle cell (VSMC) is a highly specialized entity, primarily responsible for the contraction and regulation of blood vessel diameter (Alexander & Owens 2012). Under typical conditions, VSMCs express a unique array of contractile proteins, ion channels, and signaling molecules essential for their contractile function (Durham et al., 2018) (Owens 1995). However, emerging research has elucidated that VSMCs can undergo significant phenotypic transformations, leading to pathologies such as vascular calcification. This process, characterized by the conversion of VSMCs into osteoblast-like cells, is not only prevalent but also closely linked to increased morbidity and mortality, particularly in individuals with chronic kidney disease (Leopold 2015) (Patel et al., 2019) (P. Zhang et al., 2016) (Lee et al., 2020) (Bentzon et al., 2006) (Speer et al., 2009) (Lyu et al., 2018).

The pathogenesis of vascular calcification involves multifaceted mechanisms, with recent studies emphasizing the critical role of epigenetic modifications. These alterations, including DNA methylation, non-coding RNAs, and histone modifications, are key drivers in the regulation of gene expression and chromatin structure stability (Portela & Esteller 2010). Among these, histone modifications such as acetylation, methylation, phosphorylation, and ubiquitination, catalyzed by specific

* Corresponding author. Program in Environmental and Experimental Pathology, Paulista University, São Paulo, 04026-002, São Paulo, Brazil.
** Corresponding author.
E-mail addresses: w.zambuzzi@unesp.br (W.F. Zambuzzi), dasilva.rodrigo.a@gmail.com, rodrigo.silva3@docente.unip.br (R.A.F. da Silva).

https://doi.org/10.1016/j.yexcr.2024.114311
Received 28 June 2024; Received in revised form 23 October 2024; Accepted 27 October 2024
Available online 28 October 2024

proteins, are of paramount importance (W. Fu et al., 2019) (Bannister & Kouzarides 2011). A prominent player in this context is Sirt1, a member of the histone deacetylase (HDAC) family, distinguished by its dependence on nicotinamide adenine dinucleotide (NAD+) (Winnik et al., 2015) (Guarente 2011). Sirt1 plays a pivotal role in mediating cell death/survival processes and has implications in the pathogenesis of cardiovascular diseases. In the context of vascular calcification, it primarily acts in the deacetylation of eNOS, promoting NO production and delaying VSMC senescence (Vasa et al., 2000) (Lu et al., 2020), particularly during the phase exhibiting a heightened transition to the osteogenic phenotype (Liu et al., 2013).

Despite these insights, little is known about Sirt1's involvement concerning osteoblastic differentiation genes in the context of acquiring the osteogenic phenotype. Thus, the primary objective of this study was to assess the role of histone modification in the calcification process with a specific emphasis on elucidating the regulatory role of SIRT1 in osteoblastic differentiation markers.

2. Materials and methods

2.1. Reagents and antibodies

SmGM-2 SingleQuots (Lonza, CC-4149), consisting of 0.5 mg/ml hEGF, 5 mg/ml insulin, 1 mg/mL hFGF, 50 mg/ml gentamicin/amphotericin-B, and 5 % fetal bovine serum. Lonza, based in Walkersville, MD, provided this culture supplement. Additional reagents obtained from Sigma Chemical Co. (St. Louis, MO, USA) include RIPA buffer (R0278), phosphatase inhibitor cocktail 2 (P5726), bovine serum albumin (A7906), Fluoroshield (F6057), saponin (47036), Triton X100 (9284), Resveratrol (R5010), and EX-527 (E7034). The Gotaq qPCR master mix (A6002) was procured from PROMEGA (Madison, Wisconsin, USA). Life Technologies/Molecular Probes, Inc. (Eugene, OR, USA) supplied Conjugated DNase I, High-Capacity cDNA Reverse Transcription kit, TRIzol, and phalloidin conjugated with Alexa Fluor 488. Antibodies used in the study are detailed in Table 1.

Table 1
Primary and secondary antibodies used in the study.

ANTIBODY	CODE	MW (kDa)		RESEARCH
Primary antibodies				
α-SMA	SC 53142	43	Mouse IgG	Santa Cruz Biotechnology
Runx 2	SC 101145	17	Mouse IgG	Santa Cruz Biotechnology
OTX	SC 393060	17	Mouse IgG	Santa Cruz Biotechnology
H3K9ac	#9649	17	Rabbit IgG	Cell Signaling Tecnology
H3K27ac	#8173	17	Rabbit IgG	Cell Signaling Tecnology
H3	#4620	17	Rabbit IgG	Cell Signaling Tecnology
HAT1	#41490	49	Rabbit IgG	Cell Signaling Tecnology
PCAF	#3378	93	Rabbit IgG	Cell Signaling Tecnology
HDAC1	#5356	62	Mouse IgG	Cell Signaling Tecnology
HDAC2	#5113	60	Mouse IgG	Cell Signaling Tecnology
HDCA3	#7628	49	Rabbit IgG	Cell Signaling Tecnology
p-HDAC	#3443	140	Rabbit IgG	Cell Signaling Tecnology
SIRT 1	#8469	120	Mouse IgG	Cell Signaling Tecnology
β-Actin	#3700	45	Mouse IgG	Cell Signaling Tecnology
GAPDH	#5174	37	Rabbit IgG	Cell Signaling Tecnology
Secondary antibodies				
Anti-Mouse - Alexa Fluor 594	#4408	–	IgG	Cell Signaling Tecnology
Anti-Rabbit - Alexa Fluor 594	#4412	–	IgG	Cell Signaling Tecnology
Anti-Mouse - HRP	#7076	–	IgG	Cell Signaling Tecnology
Anti-Rabbit - HRP	#7074	–	IgG	Cell Signaling Tecnology

2.2. Cell culture and in vitro model of VSMCs calcification

The human primary aorta smooth muscle cells (AoSMC - CC-2571), procured from Lonza (Walkersville, MD), were employed in this study and cultured at 37 °C in a humidified atmosphere with 5 % CO_2. The culture medium used was SmBM-type medium (Smooth Muscle Cell Meio Basal, Lonza, CC-3181), supplemented with SmGM-2 SingleQuots [0.5 mg/ml hEGF, 5 mg/ml insulin, 1 mg/ml hFGF, 50 mg/ml gentamicin/amphotericin-B, and 5 % fetal bovine serum (Lonza, CC-4149)], following the manufacturer's guidelines. For the calcification model, cells (10×10^4 cells) were seeded and allowed to reach 80 % confluence. Subsequently, they were washed in phosphate-buffered saline (PBS) and exposed to a treatment consisting of 2.7 mM calcium and 2.6 mM phosphate in DMEN containing 10 % FBS and 1 % antibiotics (penicillin and streptomycin) (Vitrocel, Campinas, SP). The cells were then maintained at 37 °C in a humidified atmosphere with 5 % CO_2 for a duration of up to 72 h.

2.3. mRNA Isolation and gene expression analysis

Total RNA extraction was conducted using the Ambion TRIzol Reagent (Life Sciences, Thermo Fisher Scientific Inc., Waltham, MA, USA), and reverse transcription was performed using the high-capacity cDNA reverse transcription kit (Applied Biosystems, Foster City, CA, USA) following the manufacturer's guidelines. Quantitative polymerase chain reaction (qPCR) was executed using a QuantStudio® 3 real-time PCR system to assess changes in mRNA expression for the genes outlined in Table 2. Real-time PCR was carried out using PowerUpTM SYBR Green Master Mix™ (Applied Biosystems, Foster City, CA, USA). Gene expression levels were normalized using a combination of three reference genes (18S, β-ACTIN, and GAPDH) through the ΔΔCT method, and results were compared with the control group.

2.4. Western blotting

Following the calcification process, protein extraction was performed using 300 μL Laemmli Buffer [SDS 4 %, glycerol 20 %, Tris-Cl (pH 6.8) 120 mM, bromophenol blue 0.02 % (w/v), and DTT 0.1 M]. Equal volumes of samples (20 μL) were loaded onto SDS-PAGE and transferred to polyvinylidene difluoride (PVDF) membranes (Millipore, Bedford, MA). The membranes were blocked in 2.5 % BSA in saline solution buffered with Tris with 0.05 % Tween 20 (TBST-A) and incubated overnight at 4 °C with the primary antibodies listed in Table 1. After washing in TBST, membranes were incubated with appropriate HRP-linked secondary antibodies (diluted at 1:5.000) in blocking buffer for 1 h. Immunoreactive bands were visualized using an enhanced chemiluminescence kit.

2.5. Confocal microscopy

For confocal microscopy analysis, glass coverslips were sterilized under UV light for 15 min and placed in 100-mm culture dishes. After the calcification treatment period (24h, 48h, 72h), cells were washed with PBS, fixed in PBS-paraformaldehyde (4 % v/v), and permeabilized in PBS containing 0.2 % Triton-X 100 and 1 % BSA at 37 °C for 30 min. The cells were then stained for 1 h with specific primary antibodies at concentrations recommended by the manufacturer. Subsequently, after

Table 2
Expression primers sequences and PCR cycle conditions.

Gene (ID)	Primer	5′- 3′ Sequence	Reactions Condicition	Product size (pb)
GAPDH (2597)	Forward	AAG GTG AAG GTC GGA GTC AA	95 °C – 8s; 58 °C – 8s; 72 °C – 8s	108
	Reverse	AAT GAA GGG GTC ATT GAT GG		
ACTB (60)	Forward	ACA GAG CCT CGC CTT TGC	95 °C – 8s; 59 °C – 8s; 72 °C – 8s	935
	Reverse	GCG GCG ATA TCA TCA TCC		
18S (106632259)	Forward	CGG ACA GGA TTGACA GAT TGA TAG C	95 °C – 8s; 58 °C – 8s; 72 °C – 8s	118
	Reverse	TGC CAG AGT CTC GTT CGT TAT CG		
TNAP (249)	Forward	CTATCCTGGCTCCGTGCTCCC	95 °C – 8s; 59 °C – 8s; 72 °C – 8s	106
	Reverse	TTGTGGTGGAGCTGACCCTT		
ENPP1 (5167)	Forward	TTT GCC GAT TGA GGA TTT TC	95 °C – 8s; 59 °C – 8s; 72 °C – 8s	221
	Reverse	CCA CTG ACG ACA TTG ACA CC		
FETUIN (26998)	Forward	GAATTCCGCTCATCCTGTTCT	95 °C - 15s; 63 °C - 30s; 72 °C - 30s	179
	Reverse	CGTGGAAATCGCAGTCTCCT		
HAT 1A (2033)	Forward	CAT CCC CAA AGA GTT GAT GG	95 °C - 15s; 60 °C - 30s; 72 °C - 30s	213
	Reverse	GCA GTG GAG AAG AAA CTG GC		
PCAF (8850)	Forward	AAACCCCCATTTGAAAAACC	95 °C - 15s; 60 °C - 30s; 72 °C - 30s	220
	Reverse	TCAGATCACGGTGGATGAAA		
HDAC 1 (3065)	Forward	TGA AGC CTC ACC GAA TCC G	95 °C - 15s; 60 °C - 30s; 72 °C - 30s	210
	Reverse	GGG CGA ATA GAA CGC AGG A		
HDAC 2 (3066)	Forward	GGA GGA GGC TAC ACA ATC CG	95 °C - 15s; 60 °C - 30s; 72 °C - 30s	195
	Reverse	TCT GGA GTG TTC TGG TTT GTC A		
HDAC 4 (9759)	Forward	AGTGGCCAGGTTATCAGTGG	95 °C - 15s; 60 °C - 30s; 72 °C - 30s	143
	Reverse	GGAGAAGAGCCGAGTGTGTC		
HDAC 6 (10013)	Forward	TCC TTG CTT GCT CTC CAG AC	95 °C - 15s; 61 °C - 30s; 72 °C - 30s	183
	Reverse	GTG CTG CGC CTA CGT AAA AG		
SIRT 1 (23411)	Forward	GAG ATA ACC TTC TGT TCG GTG ATG AA	95 °C - 15s; 61 °C - 30s; 72 °C - 30s	213
	Reverse	CGG CAA TCA AAT CTT TAA GAA TTG TTC G		
RUNX 2 (860)	Forward	CGA GAG GCA ACT CCA CGC T	95 °C - 15s; 60 °C - 30s; 72 °C - 30s	360
	Reverse	CCC GCC CCT TTC CAA GCG		
OTX (121340)	Forward	GCC GAT TAG AGC CCG AGA G	95 °C - 15s; 60 °C - 30s; 72 °C - 30s	195
	Reverse	AGG AAG AAG CTT GGA TGC		
α-SMA (946582)	Forward	AGG AGT TCC GCT CCT CTC TC	95 °C - 15s; 61 °C - 30s; 72 °C - 30s	381
	Reverse	TGG AGG CTT ACC CCG TCT TAG T		

removing the primary antibody through PBS washing, cells were stained with Alexa Fluor 488 antirabbit or mouse IgG antibody for 1 h for fluorescence analysis. For actin cytoskeleton rearrangement analyses, cells were incubated for 40 min with 4 mg/ml Alexa Fluor 488-labeled phalloidin (Invitrogen/Molecular Probes, Waltham, MA). Following additional washing, coverslips were mounted on glass slides using Fluorosield with 4′,6-Diamidine-2′-phenylindole dihydrochloride (DAPI) (Sigma, St. Louis, MO) and observed on an inverted laser scanning confocal microscope (Leica TCS SP5).

2.6. DNA extraction and methylation analysis

Total DNA purification involved extraction with phenol/chloroform/isoamyl alcohol, and the resulting DNA samples were stored at −20 °C. The extracted DNA underwent an initial treatment with T4-β- glucosyltransferase (T4-BGT; New England Biolabs, Beverly, MA), which added a glucose moiety to 5-hmeC (gDNA) for differentiation between DNA methylation and hydroxymethylation. Each sample was divided into three tubes, each containing 400 ng gDNA, and treated with 1 × nucleotide exchange (NE) buffer, 40 mM UDP glucose, and T4-BGT (1 unit) to a final volume of 40 μl. The mixture was then incubated at 37 °C for 1 h, followed by 10 min at 65 °C. Subsequently, the samples were digested with *Msp*I or *Hpa*II restriction enzymes (New England BioLabs, Beverly, MA), or H2O (control), following the manufacturer's instructions. Primers were designed on regulatory regions, including DNaseI hypersensitivity cluster sites, layered by histone modification marks, CpG regions, and transcription factor binding sites (Table 3).

2.7. Resveratrol and EX-527 preparation

Resveratrol and EX-527 were obtained from Sigma (St. Louis, MO, USA). Resveratrol is a SIRT1 stimulator (0.6 mg) was dissolved in DMEM with 10 % FBS, while EX-527, an inhibitor, was dissolved in DMSO (Sigma-Aldrich, St. Louis, MO, USA). Both compounds were prepared as 100 mM stock solutions and stored at −20 °C until later use.

2.8. Cell viability assay

A cell viability assay was conducted on AoSMCs seeded in 96-well microplates and treated with different concentrations of Resveratrol (0.375–100 μM) and the SIRT-EX 527 inhibitor (0.5–100 μM) within 24 h. Viable cells were stained with the vital MTT dye (1 mg/ml). The

Table 3
Gene methylation-specific primers sequences and PCR cycle conditions.

Gene (ID)	Primer	5′- 3′ Sequence	Reactions Condicition	Product size (pb)	Restriction enzymes sites
HDAC 1 (3065)	Forward	CAA GAT GGC GCA GAC GCA G	95 °C – 8s; 58 °C – 8s; 72 °C – 8s	160	chr x: 47.582.487 (site 1) 47.582.506 (site 2)
	Reverse	CTT GGT CTC AGC CTC GAT CT			
HDAC 2 (3066)	Forward	CCG CTC ACC GTC GTA GTA GT	95 °C – 8s; 59 °C – 8s; 72 °C – 8s	251	chr 16: 554.793.41 (site 1) 554.795.91 (site 2)
	Reverse	GTT TCC CTC AGC CCT TTT CT	95 °C – 8s; 58 °C – 8s; 72 °C – 8s	160	chr x: 47.582.487 (site 1) 47.582.506 (site 2)
HDAC 4 (9759)	Forward	CAG TAG TGG CCG TAA ACA CG			
	Reverse	ACC CAC TGC CAG TAT CCA A			
HDAC 6 (10013)	Forward	TCCTTGCTTGCTCTCCAGAC	95 °C – 8s; 59 °C – 8s; 72 °C – 8s	251	chr 16: 554.793.41 (site 1) 554.795.91 (site 2)
	Reverse	GTGCTGCGCCTACGTAAAAG			
SIRT 1 (23411)	Forward	CCG ACA ACT TGT ACG ACG AA	95 °C – 8s; 60 °C – 8s; 72 °C – 8s	160	chr x: 47.582.487 (site 1) 47.582.506 (site 2)
	Reverse	CAA CCT CAG GCC AGT AGG AG			

insoluble blue dye formed was appropriately resuspended in dimethylsulfoxide (DMSO), and cell viability was assessed by measuring absorbance in a microplate reader (SYNERGY-HTX multimode reader, Biotek, USA) at a wavelength of 570 nm. The chosen concentration for use in the study was 9 μM.

2.9. Statistical analysis

All experiments were performed at three independent times, in triplicate, and the results were expressed as mean ± standard deviation. Statistical analysis was performed *t*-test and one-way – ANOVA. Differences were considered significant at $P < 0.05$ in two-sided tests of statistical significance. Densitometric analysis of the blots was performed using Scion Image software and fluorescence intensity using LAS AF programs (Leica) and images prepared in Adobe Photoshop CS6.

3. Results

3.1. Elevated Ca^{+2} and P concentrations induce osteogenic phenotype in VSMCs

The manifestation of vascular calcification stems from alterations in muscle cells, marked by the expression of osteoblastic differentiation markers. Utilizing a well-established model for vascular calcification studies (da Silva et al., 2020), we treated AoSMC cells with a medium enriched with calcium and phosphate for 24, 48, and 72 h to induce cell calcification. Protein and gene expression analyses validated the calcifying model. As depicted in Fig. 1a, the percentage of α-SMA protein content exhibited an increase at 24h in the calcification group. At 48 and 72 h in the group exposed to the calcification medium we observed a reduction. This finding is consistent with the characterization of α-SMA as a marker of the contractile phenotype (Hinz et al., 2001). Concurrently, proteins directly associated with osteoblastic differentiation, Runx 2 and Osterix, were investigated. A decrease in Runx 2 protein content (Fig. 1b) and a significant increase in Osterix (Fig. 1c) within the calcification group compared to the control group were observed. Gene expression analysis of calcification-related genes unveiled a substantial increase at 24 and 72 h in the calcification group for Fetuin (Fig. 1d), a pivotal component in the process, as well as for TNAP and NPP1 (Fig. 1e and f), which are primarily associated with bone mineralization. These findings align with those previously reported (da Silva et al., 2020), reinforcing the transition from VSMC to the osteogenic phenotype.

3.2. Acetyltransferase enzymes in the calcification process

Previous evidence suggests that alterations in histones, specifically acetylation, methylation, and phosphorylation, play a regulatory role in the binding of specific transcription factors to DNA sequences in normal or transient cellular states (Stein et al., 2010; Josefowicz et al., 2016). To investigate whether changes in histones influence the smooth muscle cell calcification process, we examined the overall acetylation levels of lysine 9 and 27 (H3K9ac and H3K27ac), two marks linked to cardiovascular diseases, but not widely studied. Fig. 2 illustrates the gene and protein expression levels of components involved in this modification process. The gene expression of HAT and PCAF enzymes was assessed using qPCR. The results indicate an upregulation of HAT expression at 24 and 48 h in the calcified group (Fig. 2a), while PCAF expression increased only at 24 h in the same group (Fig. 2b). Protein levels were also examined, revealing that HAT levels decreased at 24 h but increased at 48 and 72 h in AoSMCs treated with a calcium and phosphate-rich medium (Fig. 2c and d). Conversely, PCAF protein levels were reduced at all three time points in this group (Fig. 2c–e). The acetylation levels of lysine 9 (H3K9ac) decreased at 24 and 48 h but increased after 72 h in

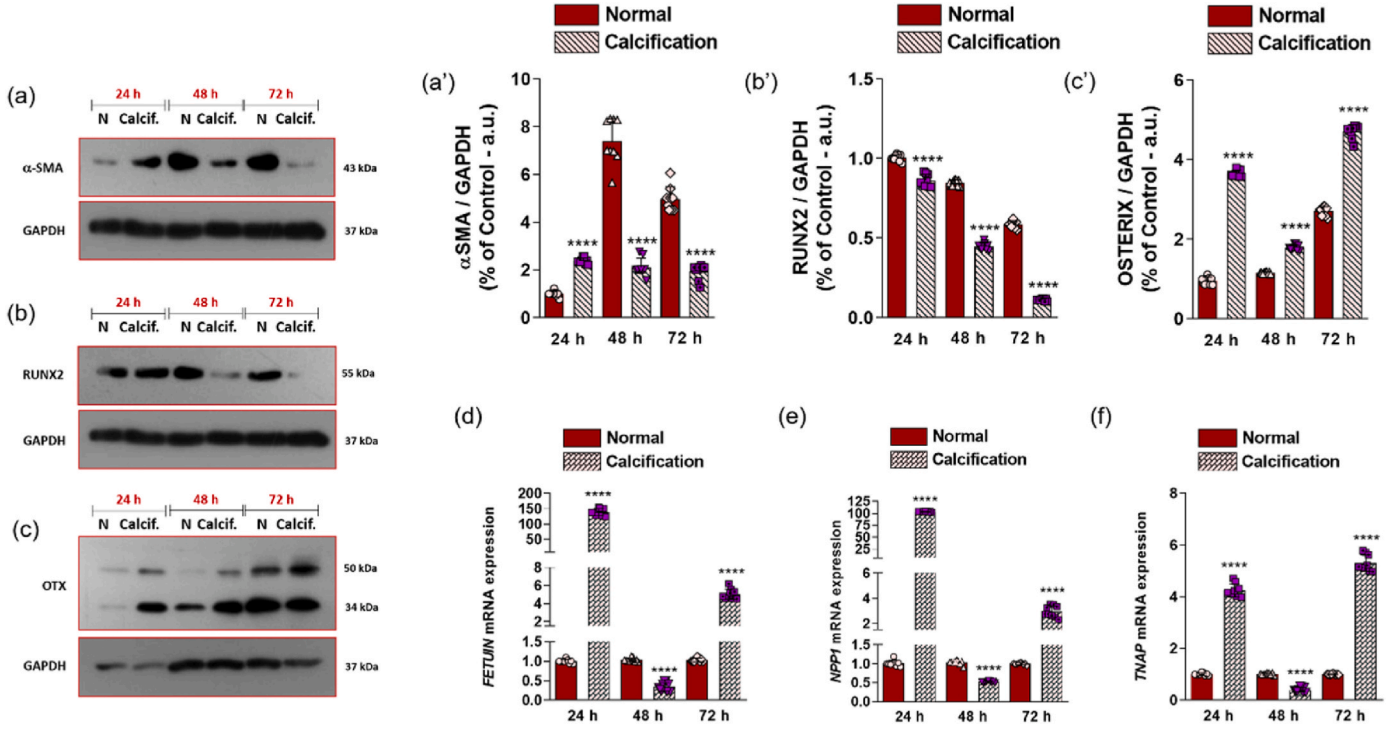

Fig. 1. Osteogenic phenotype of VSMC in overload of Ca^{+2} and P^{+}. Representative immunoblots of α-SMA (a), RUNX2 (b), and OTX (c) from AoSMC after 24, 48, and 72 h of treatment with calcification induction medium. Graphical representation of densitometric analysis of immunoblots after normalization by the application control (GAPDH) of α-SMA (a'), RUNX2 (b'), and OTX (c') proteins. Relative gene expression of FETUIN (d), NPP1 (e), and TNAP (f). Levels were determined using the cycle threshold (Ct) method and shown in a graphical format with values normalized to the value 1 assigned to the control. Results are represented as the mean ± standard deviation of three independent experiments performed in triplicate each (n = 9). *p < 0.05, **p < 0.001, and ***p < 0.0001 relative to their respective control. Immunoblot images are representative of three independent experiments.

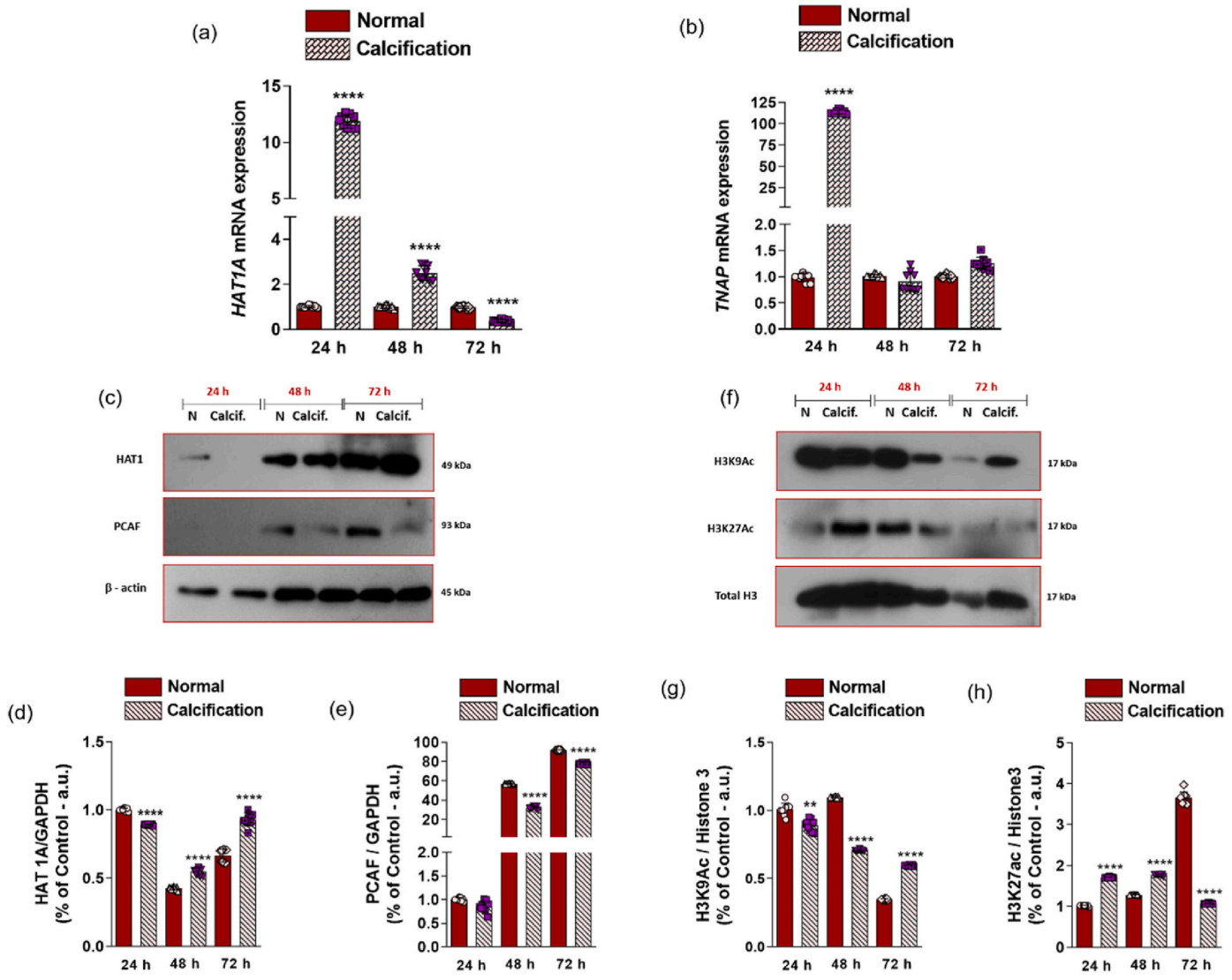

Fig. 2. Action of acetyltransferase enzymes in the calcification process. *HAT1* (a) and *PCAF* (b) gene expression was detected by qPCR analysis normalized by *18S*, *β-ACTIN* and *GAPDH* genes expression level and expressed as mean ± standard of three independent experiments performed in technical duplicate. The value for was normalized to 1. One representative immunoblot of three independent experiments is presented and densitometric analysis are expressed as the relative intensity ratio of Histone 3 total for methylation and acetylation marks and GAPDH for protein content. The results bring the notion of the variations on trimethylation profile in histone 3 (H3) at lysine 9 and 27 (f) and HAT1 and PCAF (c). Graphic representation of densitometric analysis of immunoblots after normalization by application control (β-actin) of proteins HAT1 (**d**) and PCAF (**e**) and for marks H3K9ac (**g**) and H3K27ac (**h**). The results represented as the mean ± standard deviation of three independent experiments in the AoSMC cell line, performed in triplicate each, totaling n = 9. *p < 0.05, **p < 0.001 and ***p < 0.0001 in relation to their respective control. Immunoblots images are representative of three independent experiments.

the calcification group compared to the control (Fig. 2f; g). In contrast, lysine 27 (H3K27ac) levels increased at the initial times (24 and 48h) in the calcification group and decreased at 72h (Fig. 2f; h).

A Pearson correlation analysis was performed (Fig. S1), and the inversely proportional correlations between acetyltransferase activity (HAT1 and PCAF) and global levels of H3K9ac and H3K27ac were positively significant when H3K27ac was compared with HAT at 24 and 72 h (Figs. S1a and c), with PCAF at all three time points (Fig. S1 d, e, f). H3K9ac was only positive when compared to PCAF at 24 and 72 h (Figs. S1k and l).

3.3. Balance between acetyltransferases and deacetylases modulates vascular calcification process

The equilibrium between histone acetyltransferases (HATs) and histone deacetylases (HDACs) is crucial for gene expression regulation, with HDACs being of particular interest in this process (de Ruijter et al., 2003). Our exploration aimed to unravel the involvement of these deacetylases during the muscle cell calcification event, focusing on the gene expression of different HDACs. A decrease in HDAC 1 transcripts was observed at 48 h for the calcification group, while HDAC 2 transcripts exhibited an increase at 24 and 48 h in the same group (Fig. 3a and **b**). Conversely, HDACs 4 and 6 demonstrated an upregulation in expression within the calcification group at 24 and 72h (Fig. 3c and **d**). Complementing these gene expression findings, immunofluorescence analysis and laser scanning confocal microscopy provided optical sections for each of the studied HDACs (Fig. 3e–g). The results revealed a decrease in 24 and 48h for the nuclear protein for HDAC1 (Fig. 3h) and significantly increased at 24 and 72 h in the group subjected to calcium/phosphate overload in the levels of nuclear protein for HDAC 2 (Fig. 3i). The HDAC4 nuclear content didn't show significantly differences (Fig. 3j). In contrast, a reduction in the nuclear protein quantity of HDACs 1 and 6 was observed at 24 and 48 h for the calcification group when compared to the control group (Fig. 3h and **k**,

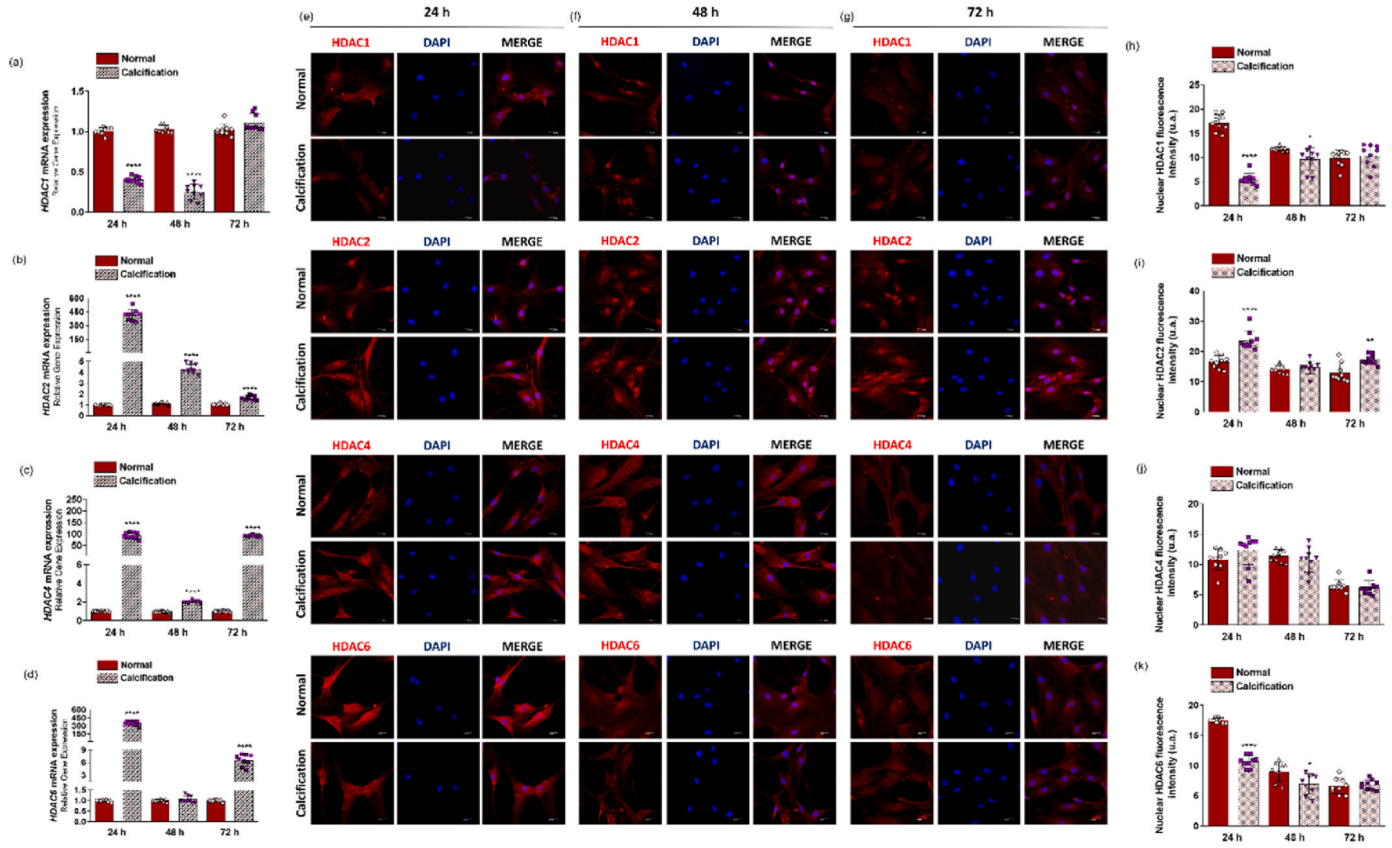

Fig. 3. Acetyltransferases and deacetylases modulate vascular calcification. Gene expression of histone deacetylase family members [HDACs (HDAC1 - a; HDAC2 - b, HDAC4 - c, and HDAC6 - d)] was detected by qPCR analysis normalized by the expression level of 18S, β-ACTIN, and GAPDH genes in AoSMC cDNA produced after RNA extraction. Subcellular localization of HDAC family members was determined by confocal microscopy analysis of HDAC1, HDAC2, HDAC4, and HDAC6 members after 24 (e), 48 (f), and 72 (g) hours, and nuclear fluorescence of HDAC1 (h), HDAC2 (i), HDAC4 (j), and HDAC6 (l) was determined using a LAS AF program. Confocal fluorescence microscopy images and gene expression results were represented as mean ± standard deviation of three independent experiments, performed in triplicates, totaling n = 9. *p < 0.05, **p < 0.001 and ***p < 0.0001 in relation to their respective controls. Bar = 50 μm.

Considering that both the activity and nuclear export of HDAC family members can be regulated by phosphorylation (de Ruijter et al., 2003) (Huynh & McKinsey, 2006), we assessed the subcellular location of the phosphorylated form of HDAC (p-HDAC). Optical sections obtained at different established time points are represented in Fig. 4 a, b, c. The quantification showed a decrease in p-HDAC in the three times (Fig. 4d). To evaluate the activity of these deacetylases, we determined the ratio between the nuclear content of p-HDAC and the total protein content of HDACs 1, 2, 4 and 6.

The data revealed a predominance of the phosphorylated form of HDAC1 (increased ratio p-HDAC/HDAC1) in the calcified cell group after 24h of treatment (Fig. 4e). At 24 and 48 h, a significant decrease was observed in the calcification group for the p-HDAC/HDAC2. (Fig. 4f). The p-HDAC/HDAC4 ratios showed a significant increase at 48 and 72 h (Fig. 4g). In the p-HDAC/HDAC6 ratio we observed an increase at 72h (Fig. 4h). Based on the data, we investigated whether these enzymes were epigenetically regulated during the transition of the calcification phenotype in these VSMCs. The data revealed that the modulation of the differential expression of HDACs did not occur via DNA methylation, as shown in Fig. S2.

3.4. SIRT1 involvement during the calcifying acquisition phenotype of VSMCs

Examining SIRT1, a class III deacetylase that acts beyond histones and plays a protective role in preventing muscle cell calcification (Li et al., 2016; D'Onofrio et al., 2018; Nasiri et al., 2018), we evaluated its gene expression during treatment with high levels of calcium/phosphate. A significant increase in SIRT1 transcripts was observed compared to the control group (Fig. 5a) at the three times. Protein contentof SIRT1 in the calcification group increased at 48 and 72h, with a reduction noted at 24h (Fig. 5b and c). Methylation analysis of the SIRT1 promoter gene indicated hypomethylation in the calcification group after calculating the ratio of 5hmeC and 5meC (Fig. 5d–f), suggesting regulation via DNA methylation. This was corroborated by Pearson correlations showing an inverse proportion between the methylation level of the SIRT1 promoter and the transcript expression at various time points of treatment (Fig. 5g, h, i). Immunofluorescence analysis using a specific antibody for SIRT1 revealed a decrease in nuclear translocation in response to muscle cell calcification (Fig. 5k–j).

3.5. Regulation of SIRT via DNA methylation in muscle cell calcification

Given its protective effect on vascular calcification (P. Zhang et al., 2016) (Tomayko et al., 2014), and building upon the results presented in the previous figure, we sought to investigate how cells treated with high levels of calcium/phosphate would respond in the presence of Resveratrol, a component abundantly present in grapes, wine, peanuts, soy, and fruits (Galiniak et al., 2019) and a SIRT stimulator, and in the presence of EX-527, a selective inhibitor of SIRT, during the 72h period.

In this section, the analyzed groups were divided into control, calcification, resveratrol, and EX-527. Gene expression analyses of markers used to validate the model corroborate those presented in the first figure of this work. It was observed a reduction of α-SMA transcripts in the calcification group, together with the treatment of both compounds, and an increase in transcripts in this same group for the RUNX 2,

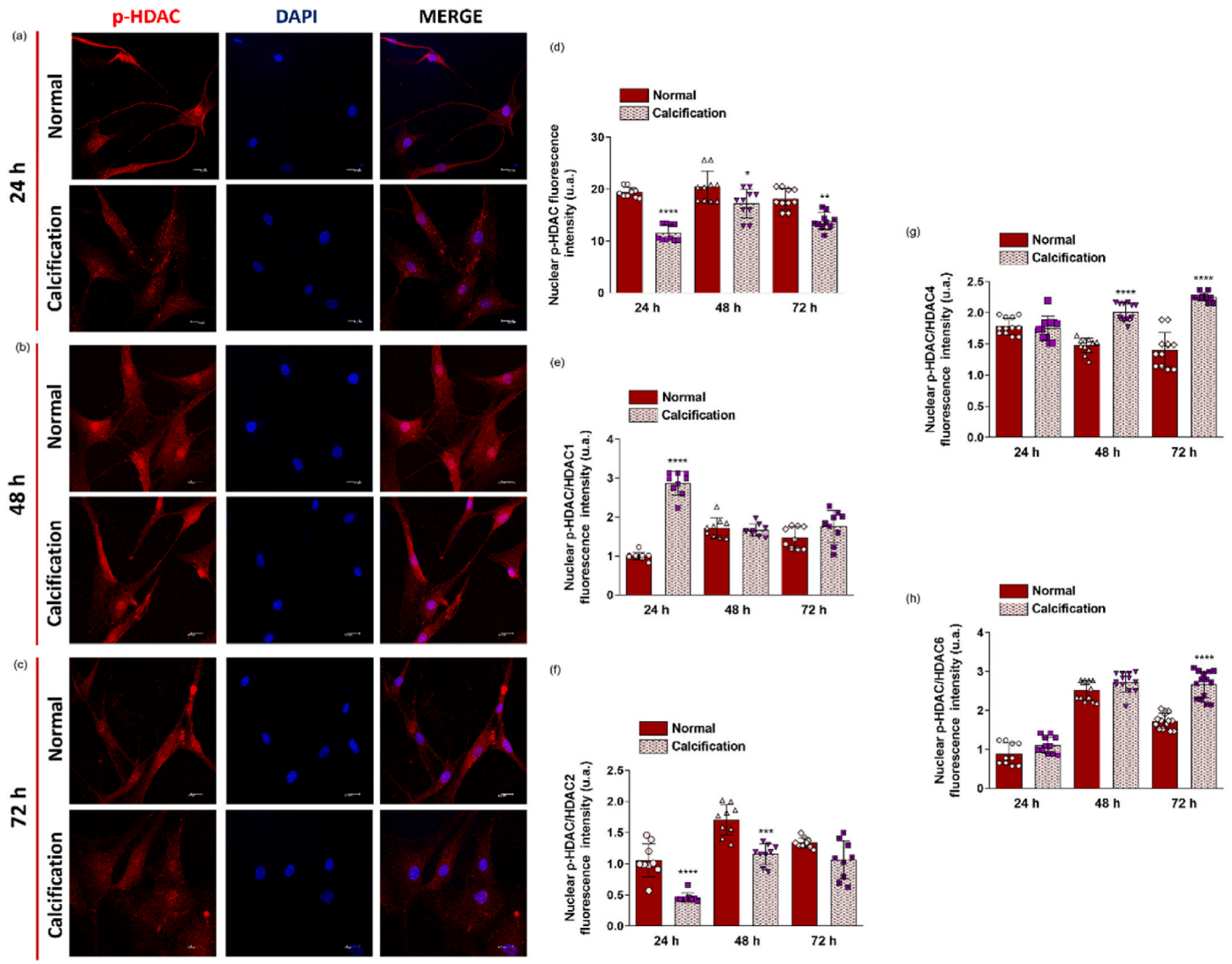

Fig. 4. The subcellular localization of p-HDAC members was determined by confocal microscopy analysis in AoSMC after 24 (**a**), 48 (**b**) and 72 (**c**) hours. The nuclear p-HDAC fluorescence was determined using a LAS AF programs (**d**). Images of fluorescence confocal microscopy are representative of three independent experiments. Graphic representation of fluorescence ratio between the nuclear fluoresce intensity of HDAC1 (**e**), HDAC2 (**f**), HDAC4 (**g**) and HDAC6 (**h**) versus the p-HDAC nuclear fluoresce intensity after 24, 48, and 72 h was determined. The results of gene expression represented as the mean ± standard deviation of three independent experiments performed in triplicate each (n = 9). *p < 0.05, **p < 0.001 and ***p < 0.0001 in relation to their respective control. Bar = 50 μm.

OTX, FETUIN, NPP1, and TNAP genes involved in the osteogenesis process (Fig. 6a–f). Immunoblotting analyses revealed that the protein content of RUNX 2 decreased when compared to the other groups, mainly in the Resveratrol and EX-527 groups (Fig. 6i).

Protein content and SIRT1 gene expression were evaluated in the different groups. The amount of protein in the EX-527 calcification group was reduced when compared to the other groups (Fig. 6j). The amount of transcripts showed an increase in SIRT1 in the resveratrol and EX-527 groups when compared to the others, and only in the calcified group with EX-527, a significant decrease was noticed (Fig. 6g). Concomitant to these analyses, we investigated the methylation of the SIRT1 promoter, and as seen in Fig. 6h, the calcification, resveratrol, EX-527, and calcified groups treated with both compounds underwent hypomethylation compared to the control group, suggesting once again that this process in the muscle cell may be happening via DNA methylation. This is further highlighted in Pearson's correlations, where the correlation of gene expression and the percentage of the methylation promoter gene was analyzed (Fig. 6l–p). A brief summary of the data found in this work is shown in Fig. 7.

4. Discussion

Vascular calcification (VC) represents a complex and active process, where vascular smooth muscle cells (VSMCs) undergo a phenotypic transition, shifting from a contractile state to a calcifying one. This paradigm shift challenges the traditional view of VC as a passive consequence of VSMC death, emphasizing the need for a deeper understanding of the molecular mechanisms driving this intricate process. Our study sought to unravel the molecular intricacies underpinning VSMC calcification, exploring established biomarkers and delving into the realm of epigenetic regulation. The shift from a contractile to a calcifying phenotype was evident through the downregulation of smooth muscle markers, such as α-SMA, at 48 and 72 h. (D.-H. Kwon et al., 2020; J. Zhang et al., 2014; Villa-Bellosta et al., 2011). Intriguingly, our data revealed a nuanced temporal regulation of α-SMA, with an initial surge up to 24 h, possibly representing a compensatory mechanism to maintain the contractile phenotype in response to calcifying stimuli. Subsequently, a significant decline in α-SMA levels occurred, indicative of the evolving phenotypic shift. This aligns with observations by Steitz et al., emphasizing the dynamic nature of VSMC

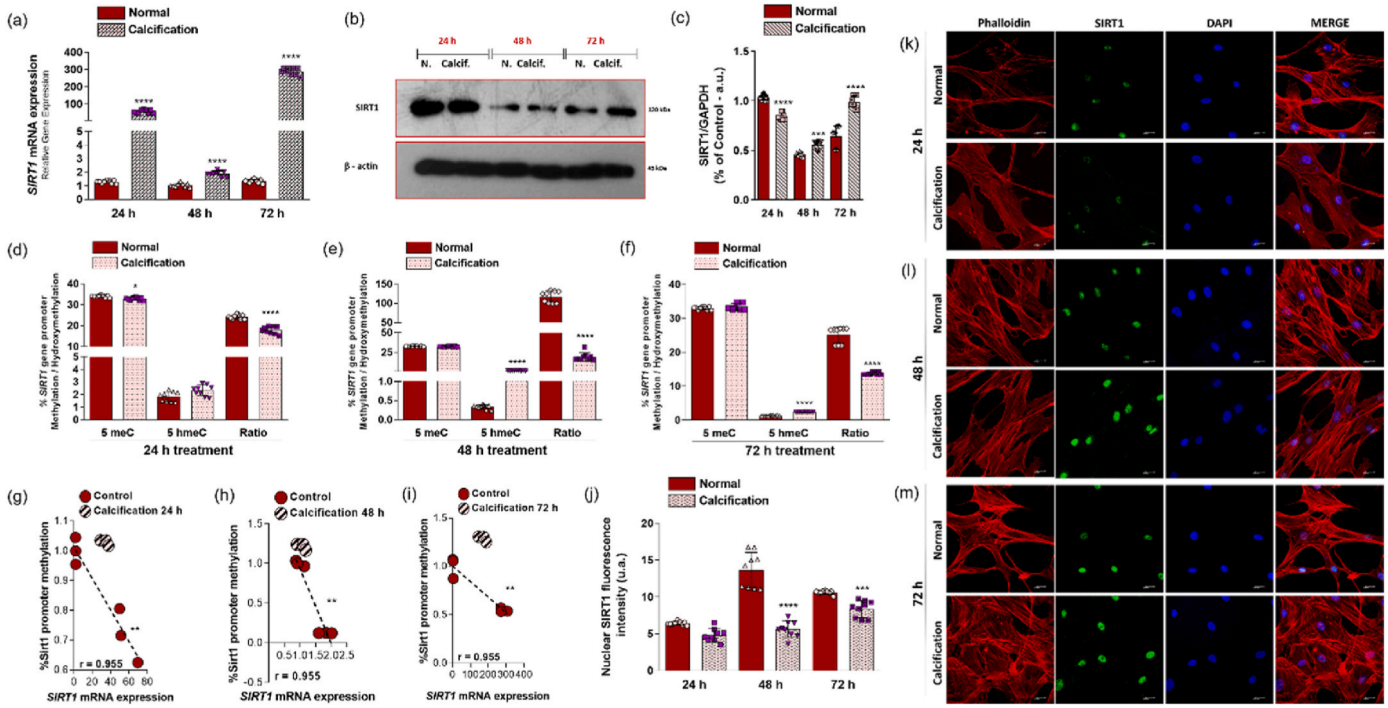

Fig. 5. Sirt action on vascular calcification SIRT. *SIRT1* gene expression (**a**) and protein content (**b**) in AoSMC exposed a medium with overload the calcium and phosphate. Graphic representation of densitometric analysis of SIRT1 immunoblot after normalization by application control (β-actin) (**c**). *SIRT1* gene promoter methylation/hydroxymethylation patterns after 24 (**d**), 48 (**e**) and 72 (**f**) hours. Correlation analysis between gene promoter DNA methylation/hydroxymethylation pattern and expression genic after 24 (**g**). 48 (**h**) and 72 (**i**) h. Significant positive correlation between r = 0.683 and 1. The nuclear SIRT1 fluorescence intensity (**j**) was determined by confocal microscopy using a LAS AF programs after 24 (**k**), 48 (**l**) and 72 (**m**) hours. Gene expression and gene promoter methylation was determined by qPCR analysis. The results of gene expression represented as the mean ± standard deviation of three independent experiments, n = 9. *p < 0.05, **p < 0.001 and ***p < 0.0001 in relation to their respective control. Bar = 50 μm.

phenotypic changes during prolonged exposure to calcifying conditions (Steitz et al., 2001). In the same samples, we also observed the simultaneous upregulation of osteogenic markers, including BMPs, RUNX2, osteocalcin, TNAP, and NPP1. These findings are consistent with previous studies highlighting the coordinated molecular changes involved in VSMC calcification.

Noteworthy among our findings is the upregulation of osterix (SP-7), a transcription factor typically associated with osteogenesis, suggesting its pivotal role in driving the transdifferentiation of VSMCs during calcification. This aligns with emerging evidence proposing SP-7 as a key mediator in the phenotypic switch of VSMCs (Radtke et al., 2015; Valenzuela et al., 2013). Furthermore, the involvement of Fetuin A, NPP1, and TNAP underscores their significance in the intricate process of VSMC calcification (Steitz et al., 2001; Kay et al., 2016; Bolean et al., 2017; Derradi et al., 2019).

Turning our attention to epigenetic regulation, we probed into histone modifications, specifically acetylation. Many histone acetylation sites have been suggested to be associated with heart diseases [1]. The acetylation state of lysine residues is determined by the dynamic control of histone acetyltransferases (HATs) and histone deacetylases (HDACs) [2,3]. The predominantly examined histone acetylation sites are H3 and H4. The acetylation positions on histones H3 and H4 include H3K4, H3K9, H3K14, H3K18, H3K23, H3K27, H3K36, H3K56, H4K5, H4K8, H4K12, H4K16, and H4K20 [4,5]. Several studies have indicated that p300-mediated H3K9 acetylation leads to cardiomyocyte hypertrophy [4,6,7]. Inhibition of HAT activity results in a decrease in H3K9 acetylation [8,9]. This was demonstrated as the data presented here emphasized the regulation of HAT1A and H3K9Ac in calcifying VSMCs. This dynamic control was further supported by Pearson correlation, highlighting the connection between acetylation and VSMC calcification. Additionally, there are reports linking H3K27 acetylation with cardiac diseases, although its association is not as prominent as that of H3K9 acetylation [10]. Histone deacetylases (HDACs) reverse the acetylation of histones by HATs, restoring histone lysine to its original unacetylated state [11]. There are four classes of HDACs, all associated with proteins that exhibit low substrate specificity. These proteins promote chromatin condensation through histone deacetylation, restricting access to DNA and suppressing transcription [10,12]. Our data point to alterations of HDACs 4 and 6, which emerged as important participants in VSMC calcification, exhibiting enhanced phosphorylation and nuclear translocation. Some authors point out that HDAC6 is involved in the process of tubulin deacetylation, in addition to acting on myofibrillar stiffness and skeletal muscle atrophy in individuals with cardiovascular diseases [13,14]. Despite the general upregulation of HDACs at the transcriptional level, the phosphorylated and translocated forms of HDACs 4 and 6 highlight their active participation in the calcification process.

SIRT1 is a widely studied member of the NAD + -dependent class III deacetylase family, recognized for its potential protective effects against cardiovascular diseases [15]. Its role in preventing calcification has been previously acknowledged and documented by researchers such as P. Zhang et al. (2016) and Tomayko et al. (2014). SIRT1 has been identified as a positive regulator of the osteoblast transcription factor RUNX2 [16]. Under high glucose conditions, reduced SIRT1 expression led to increased acetylation of the RUNX2 promoter region, thereby promoting the osteogenic differentiation of VSMCs [17]. However, little is known about its activation during calcification, prompting a deeper investigation into the epigenetic regulation of this protein's promoter in this study. Our analysis of SIRT1's role revealed a dynamic modulation of its expression during VSMC calcification. These findings provide new insights into its regulatory function. The observed hypomethylation of the SIRT1 promoter under calcification conditions suggests a potential epigenetic mechanism influencing its expression. Correlation analyses further support an inverse relationship between promoter methylation and SIRT1 expression, highlighting the complex interplay between

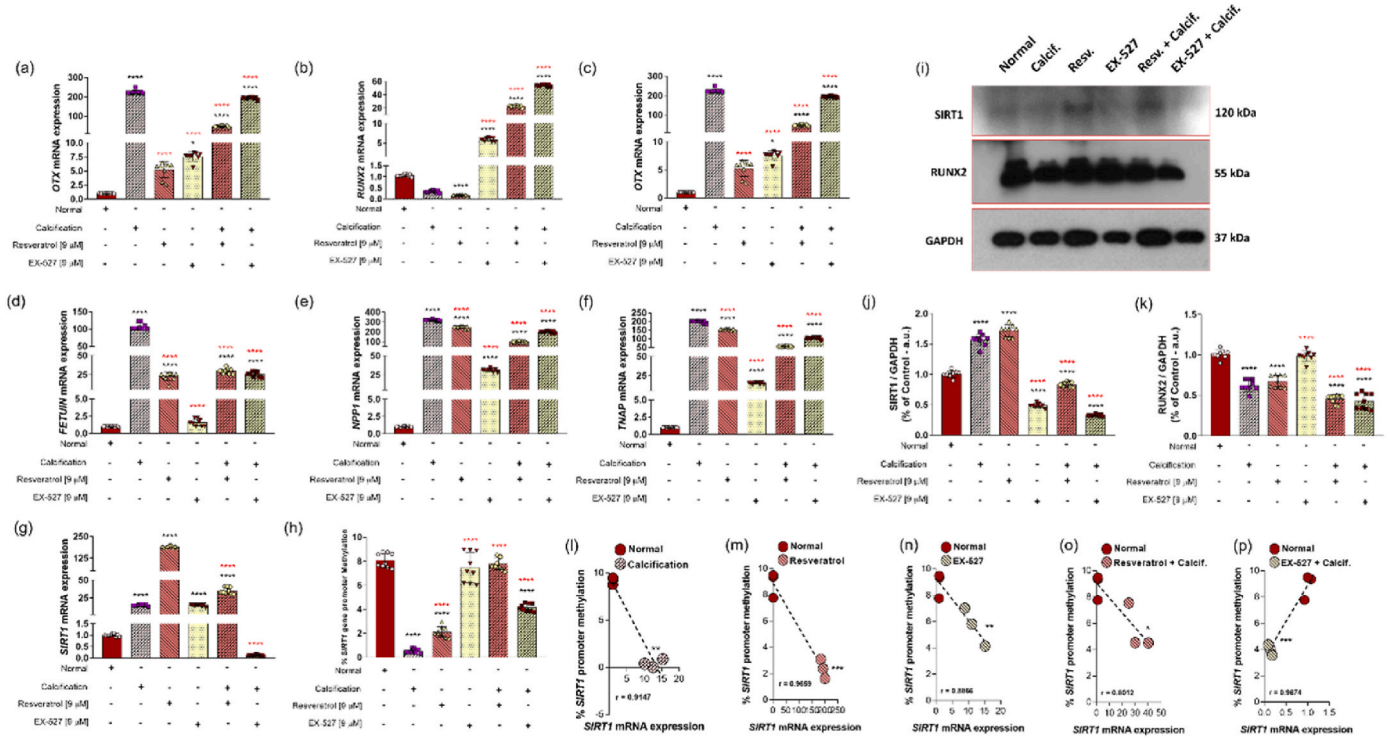

Fig. 6. Sirt agonist and antagonist acting on vascular calcification. Relative gene expression of proteins *α-SMA* (**a**), *RUNX2* (**b**), *OTX* (**c**), *FETUIN* (**d**), *NPP1* (**e**), *TNAP* (**f**) and *SIRT1* (**g**) after 24 h of treatment with a medium that induces the calcification process associated or not with the positive (resveratrol) and negative (EX527) regulator of SIRT1. Representative immunoblots of SIRT1 and RUNX2 (**i**). Graphic representation of densitometric analysis of SIRT1 (**j**) and RUNX2 (**k**) immunoblot after normalization by application control (GAPDH). *SIRT1* gene promoter methylation/hydroxymethylation patterns in human AoSMCs were determined by qPCR using genomic DNA previously treated by endonucleases T4-BGT, followed by *Msp*I and *Hpa*II after 24 h of induction of the in vitro model calcification (**h**). Correlation analysis between *SIRT1* gene promoter methylation and *SIRT1* gene expression (**l, m, n, o, p**). The mRNA was determined using the cycle threshold (Ct) method and shown in a graphical format with normalized values as a function of the control assigned value 1. The results represented as the mean ± standard deviation of three independent experiments. *$p < 0.05$, **$p < 0.001$ and ***$p < 0.0001$ in relation to their respective control. Immunoblots images are representative of three independent experiments. * black - compared to the Normal group; * red - compared to the Calcification group. Significant positive correlation between $r = 0.683$ and 1.

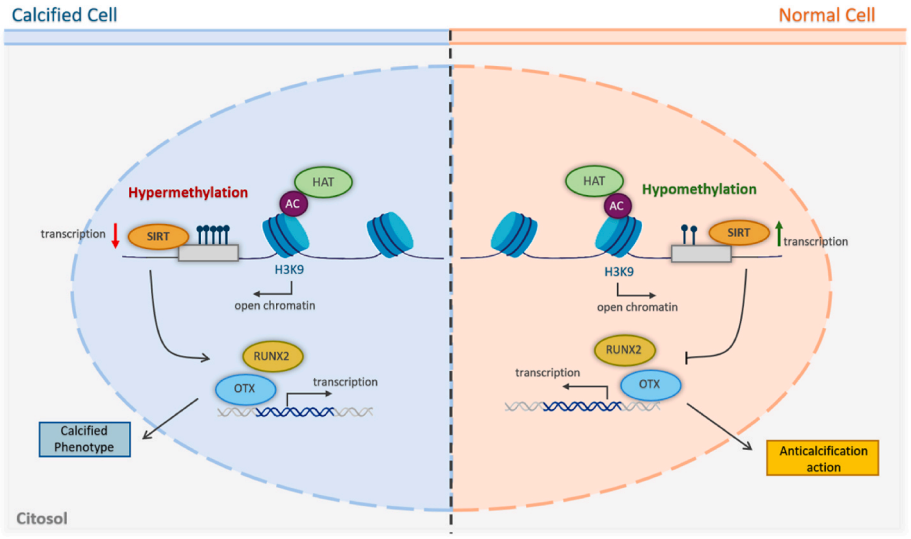

Fig. 7. A schematic overview of the molecular impacts of histone acetylation and SIRT1 methylation on vascular calcification is presented. Our study shows that histone modifications, particularly the acetylation at the H3K9ac mark, are actively involved in promoting vascular calcification. When these H3 histone markers are acetylated, the chromatin structure loosens, exposing the DNA to processes like methylation. Additionally, we emphasize that SIRT1 has a protective effect against vascular calcification, as its overexpression results in reduced levels of the RUNX2 protein. This overexpression of SIRT1 is regulated by hypomethylation at the gene's promoter region, indicating that SIRT1's activation, and thus its protective function, is driven by changes in DNA methylation.

epigenetic modifications and SIRT1 regulation in VSMC calcification. To further explore the regulatory mechanisms, we introduced Resveratrol, a SIRT1 activator, and EX-527, a SIRT1 inhibitor, during the calcification process. Interestingly, both compounds demonstrated distinct effects on gene expression markers linked to osteogenesis, underscoring the critical role of SIRT1 in determining VSMC fate. Notably, the hypomethylation of the SIRT1 promoter in the presence of these compounds suggests an epigenetic regulatory axis that modulates SIRT1 expression, potentially downregulating on osteogenic markers (RUNX2 and OTX) and thereby inhibiting calcification.Finally, Fig. 7 presents a summary of the key findings. This study demonstrates the role of epigenetic markers, particularly histone modifications like H3K9ac acetylation, and confirms SIRT1's protective effect against calcification, while also offering insights into its gene activation through DNA methylation. Our research enhances the understanding of the molecular mechanisms underlying VSMC calcification, highlighting the interaction between traditional biomarkers, histone modifications, and SIRT1's regulatory function. Decoding these complex relationships paves the way for targeted strategies to prevent and treat vascular calcification, a major challenge in clinical practice.

CRediT authorship contribution statement

Geórgia da Silva Feltran: Writing – review & editing, Writing – original draft, Validation, Methodology, Investigation, Data curation, Conceptualization. **Emerson Araújo Alves dos Santos:** Writing – review & editing, Writing – original draft, Methodology, Formal analysis. **Amanda Fantini de Camargo Andrade:** Data curation, Investigation, Methodology, Writing – original draft, Writing – review & editing. **Willian Fernando Zambuzzi:** Writing – review & editing, Writing – original draft, Supervision, Resources, Funding acquisition. **Rodrigo Augusto Foganholi da Silva:** Writing – review & editing, Writing – original draft, Validation, Investigation.

Declaration of competing interest

The authors declare that they have no known competing financial interests or personal relationships that could have appeared to influence the work reported in this paper.

Acknowledgements

We are grateful to Fundação de Amparo à Pesquisa do Estado de São Paulo (FAPESP) for their invaluable financial support (grant #2014/22689-3, #2019/26854-2, and #2019/22255-7).

Appendix A. Supplementary data

Supplementary data to this article can be found online at https://doi.org/10.1016/j.yexcr.2024.114311.

Data availability

Data will be made available on request.

References

[1] Jian Qin, Ningning Guo, Jingjing Tong, Zhihua Wang, Function of histone methylation and acetylation modifiers in cardiac hypertrophy, J. Mol. Cell. Cardiol. 159 (2021) 120–129.
[2] Zihang Huang, et al., Metabolic substrates, histone modifications, and heart failure, Biochimica et biophysica acta. Gene regulatory mechanisms 1866 (1) (2023) 194898.
[3] Yihang Jing, Xin Li, Zheng Liu, David Li Xiang, Roles of negatively charged histone lysine acylations in regulating nucleosome structure and dynamics, Front. Mol. Biosci. 9 (2022) 899013.
[4] Masafumi Funamoto, Masaki Imanishi, Koichiro Tsuchiya, Yasumasa Ikeda, Roles of histone acetylation sites in cardiac hypertrophy and heart failure, Frontiers in cardiovascular medicine 10 (2023) 1133611.
[5] Maria Shvedunova, Asifa Akhtar, Modulation of cellular processes by histone and non-histone protein acetylation, Nat. Rev. Mol. Cell Biol. 23 (5) (2022) 329–349.
[6] Masafumi Funamoto, et al., Pyrazole-curcumin suppresses cardiomyocyte hypertrophy by disrupting the CDK9/CyclinT1 complex, Pharmaceutics 14 (6) (2022).
[7] Yoichi Sunagawa, et al., Curcumin and its demethoxy derivatives possess P300 HAT inhibitory activity and suppress hypertrophic responses in cardiomyocytes, J. Pharmacol. Sci. 136 (4) (2018) 212–217.
[8] Shuo Li, et al., Anacardic acid attenuates pressure-overload cardiac hypertrophy through inhibiting histone acetylases, J. Cell Mol. Med. 23 (4) (2019) 2744–2752.
[9] Bohui Peng, et al., JNK signaling-dependent regulation of histone acetylation are involved in anacardic acid alleviates cardiomyocyte hypertrophy induced by phenylephrine, PLoS One 16 (12) (2021) e0261388.
[10] Timothy A. McKinsey, Thomas M. Vondriska, Yibin Wang, Epigenomic regulation of heart failure: integrating histone marks, long noncoding RNAs, and chromatin architecture, F1000Research 7 (2018).
[11] Edward Seto, Minoru Yoshida, Erasers of histone acetylation: the histone deacetylase enzymes, Cold Spring Harbor Perspect. Biol. 6 (4) (2014) a018713.
[12] Yu Han, Jiali Nie, Dao Wen Wang, Li Ni, Mechanism of histone deacetylases in cardiac hypertrophy and its therapeutic inhibitors, Frontiers in cardiovascular medicine 9 (2022) 931475.
[13] Ying-Hsi Lin, et al., HDAC6 modulates myofibril stiffness and diastolic function of the heart, J. Clin. Invest. 132 (10) (2022).
[14] Atsushi Sanbe, et al., Modification of cardiac disease by transgenically altered histone deacetylase 6, Biochem. Biophys. Res. Commun. 631 (2022) 48–54.
[15] Shuangshuang Wang, Siwang Hu, The role of sirtuins in osteogenic differentiation of vascular smooth muscle cells and vascular calcification, Frontiers in cardiovascular medicine 9 (2022) 894692.
[16] Kayvan Zainabadi, Cassie J. Liu, Guarente Leonard, SIRT1 is a positive regulator of the master osteoblast transcription factor, RUNX2, PLoS One 12 (5) (2017) e0178520.
[17] F. Bartoli-Leonard, et al., Suppression of SIRT1 in diabetic conditions induces osteogenic differentiation of human vascular smooth muscle cells via RUNX2 signalling, Sci. Rep. 9 (1) (2019) 878.